Entanglement entropy and computational complexity of the periodically driven Anderson impurity model

Zhuoran He and Andrew J. Millis

Phys. Rev. B **99**, 205138 — Published 22 May 2019

DOI: 10.1103/PhysRevB.99.205138

Entanglement entropy and computational complexity of the periodically driven Anderson impurity model

Zhuoran He[1] and Andrew J. Millis[1,2]

[1] *Department of Physics, Columbia University, New York, New York 10027, USA*
[2] *Center for Computational Quantum Physics, The Flatiron Institute, New York 10010, USA*

We study the growth of entanglement entropy and bond dimension with time in density matrix renormalization group simulations of the periodically driven single-impurity Anderson model. The growth of entanglement entropy is found to be related to the ordering of the bath orbitals and to the relation of the driving period T to the convergence radius of the Floquet-Magnus expansion. Ordering the bath orbitals by their Floquet quasi-energy is found to reduce the exponential growth rate of the computation time at intermediate driving periods, suggesting new ways to optimize matrix product state calculations of driven systems.

PACS numbers: 71.27.+a, 71.10.w, 71.15.m

I. INTRODUCTION

The control of strongly correlated electron systems via laser-induced oscillating electric fields is an active area of current research [1–5], raising fundamental questions related to the dynamics of driven strongly correlated models, in particular the time evolution of systems with time-dependent Hamiltonian parameters. The Anderson impurity model (AIM) [6] of a correlated orbital coupled to a noninteracting bath is of fundamental physical interest as perhaps the simplest nontrivial interacting electron model and is important as an auxiliary model in the dynamical mean-field theory of correlated electron physics [7–9]. The development of efficient methods to calculate the nonequilibrium properties of interacting electron models such as the Anderson impurity model is a key challenge [10–13].

The density matrix renormalization group (DMRG) [14–16] is widely used as a solver for the Anderson impurity model [17–19]. In DMRG, the system's wave function is represented by a matrix product state (MPS), and the key issue is the growth of entanglement entropy of the MPS with simulation time. In a previous study [20] we introduced a 4-MPS variant of DMRG to study the "quench" physics of the Anderson model, i.e., the time evolution following an instantaneous change of interaction and/or hybridization parameters from one set of constant values to another. We found that different arrangements of bath orbitals could dramatically affect the growth of entanglement entropy, and a particular arrangement (the "star geometry" [19], associated with a proper energy ordering of bath orbitals) led to a very slow (logarithmic) growth of entanglement entropy, enabling simulations of the long-time behavior at a computational cost that grew only polynomially with the simulation time. In this paper, we move beyond the quench physics to study the real-time dynamics of the periodically driven single-impurity Anderson model (SIAM).

We generalize the 4-MPS method introduced in our previous work [20]. In this method the system's wave function is represented as a sum of four terms, each of which is the direct product of one of the four states of the impurity ($|0\rangle, |\uparrow\rangle, |\downarrow\rangle, |\uparrow\downarrow\rangle$) and an MPS of the bath. We find that there is a critical driving period T_c, namely 2π over the band width of the bath density of states, such that if the driving period $T < T_c$, the driven system is as easy to simulate as a quenched SIAM, while if $T > T_c$, the simulations become much more expensive. The period T_c is related to the convergence radius of the Magnus expansion [21–24]. For driving periods $T > T_c$, computations with standard orderings of the bath orbitals lead to linear growth of entanglement entropy with time, implying an exponential increase of computational cost with simulation time. We find that an ordering of the bath orbitals exists, which we call quasi-energy ordering, such that the asymptotic entanglement entropy growth is slow (logarithmic in time, for the noninteracting model, and with a small linear coefficient for the interacting model), enabling in principle simulations out to very long times. However, the initial transient growth of entropy for this bath ordering can be very rapid before the asymptotic limit is reached, which limits the maximum simulation times reachable in practice.

The rest of the paper is organized as follows. Section II describes the driven SIAM we solve and the application of the 4-MPS method [20] to the driven model. Sec. III presents results obtained for the driven noninteracting SIAM to illustrate the asymptotics of entropy growth in different parameter regimes and determine the complexity diagram. In Sec. IV, we simulate the interacting SIAM, show some physical results and discuss entropy growth. Section V is a conclusion and summary.

II. THEORY AND METHOD

We consider a single-impurity Anderson model (SIAM) with time-dependent model parameters. The general form of the model Hamiltonian $H(t)$ is

$$H(t) = H_d(t) + H_{\rm bath}(t) + H_{\rm mix}(t), \qquad (1)$$

with

$$H_d(t) = \sum_\sigma \varepsilon_d(t) n_{d\sigma} + U(t)(n_{d\uparrow} - \tfrac{1}{2})(n_{d\downarrow} - \tfrac{1}{2}), \quad (2)$$

$$H_{\rm bath}(t) = \sum_{k\sigma} \varepsilon_k(t)\, c^\dagger_{k\sigma} c_{k\sigma}, \quad (3)$$

$$H_{\rm mix}(t) = \sum_{k\sigma} V_k(t)\, d^\dagger_\sigma c_{k\sigma} + \text{h.c.}, \quad (4)$$

where $n_{d\sigma} = d^\dagger_\sigma d_\sigma$ and $\sigma = \uparrow, \downarrow$ is the spin label. We use the interaction picture with respect to $H_0(t) \equiv H_d(t) + H_{\rm bath}(t)$, so $H_{\rm mix}(t)$ becomes

$$\begin{aligned} \hat{H}_{\rm mix}(t) &= U_0(0,t)\, H_{\rm mix}(t)\, U_0(t,0) \\ &= \sum_{k\sigma} V_k(t) \hat{d}^\dagger_\sigma(t) \hat{c}_{k\sigma}(t) + \text{h.c.}, \end{aligned} \quad (5)$$

where $U_0(t,0) = \mathcal{T} e^{-i\int_0^t H_0(t')dt'}$ is the time-ordered unitary evolution from 0 to t due to $H_0(t)$ and $U_0(0,t) = [U_0(t,0)]^\dagger$. Since $H_0(t)$ does not couple the d-orbital to the bath, each bath orbital evolves independently in the interaction picture:

$$\hat{c}_{k\sigma}(t) = c_{k\sigma}\, e^{-i\int_0^t \varepsilon_k(t')dt'}, \quad (6a)$$

and the d-orbital evolves according to

$$\hat{d}_\sigma(t) = d_\sigma\, e^{-i\int_0^t [\varepsilon_d(t') + U(t')(n_{d\bar\sigma} - \frac{1}{2})]dt'}, \quad (6b)$$

with $\bar\sigma$ denoting the opposite spin of σ. Notice that $\hat{n}_{d\bar\sigma}(t) = n_{d\bar\sigma}$ does not evolve in the interaction picture of $H_0(t)$ and that $n_{d\bar\sigma}$ commutes with d_σ, which together lead to Eq. (6b).

As in the 4-MPS scheme developed in our previous work [20], the wave function $|\Psi(t)\rangle$ is represented as

$$|\Psi(t)\rangle = \sum_i c_i(t)\, |i\rangle_d \otimes |\Psi_i(t)\rangle_{\rm bath}, \quad (7)$$

where i sums over the 4 impurity states $|0\rangle$, $|\uparrow\rangle$, $|\downarrow\rangle$, and $|\uparrow\downarrow\rangle$, and each $|\Psi_i(t)\rangle_{\rm bath}$ is a matrix product state. The wave function $|\Psi_i(t)\rangle$ is evolved according to

$$|\Psi(t+\Delta t)\rangle \approx e^{-i\tilde{H}_{\rm mix}(t+\frac{\Delta t}{2})\Delta t} |\Psi(t)\rangle, \quad (8)$$

with the exponential Taylor expanded to 4th order in Δt to ensure good unitarity. The time-averaged Hamiltonian $\tilde{H}_{\rm mix}(t)$ in a time step Δt is

$$\begin{aligned} \tilde{H}_{\rm mix}(t) &\equiv \frac{1}{\Delta t} \int_{t-\Delta t/2}^{t+\Delta t/2} \hat{H}_{\rm mix}(t')dt' \\ &= \sum_{k\sigma} \tilde{V}_{k\sigma}(t) d^\dagger_\sigma c_{k\sigma} + \text{h.c.}, \end{aligned} \quad (9)$$

with effective hybridization given by

$$\begin{aligned} \tilde{V}_{k\sigma}(t) \approx V_k\, e^{i\int_0^t [\varepsilon_d(t') + U(t')(n_{d\bar\sigma} - \frac{1}{2}) - \varepsilon_k(t')]dt'} \\ \times\ \text{sinc}\left(\tfrac{\varepsilon_d(t) + U(t)(n_{d\bar\sigma} - 1/2) - \varepsilon_k(t)}{2} \Delta t\right). \end{aligned} \quad (10)$$

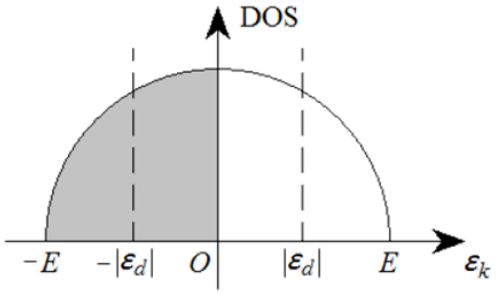

FIG. 1. The density of states of the bath orbitals ε_k. We consider a semicircle DOS with a half band width E. The bath is initially half-filled, and the d-orbital energy $\varepsilon_d = \pm|\varepsilon_d|$ oscillates between the two values shown every half driving period $T/2$ across the Fermi level.

The Hamiltonian $\tilde{H}_{\rm mix}(t)$ is represented by a matrix product operator (MPO) with bond dimension 2 that acts on the wave function in 4 MPSs [20].

We now specify the specific model we study. In the Schrödinger picture, the $\mathcal{N} \to \infty$ bath orbitals have time-independent energies $\varepsilon_k(t) = \varepsilon_k$ with a semicircular density of states (DOS) shown in Fig. 1 and time-independent and equal hybridization amplitudes $V_k(t) = V/\sqrt{\mathcal{N}}$ to the impurity d-orbital. The Hubbard U on the d-orbital is also fixed. The only time-dependent quantity is the d-orbital energy, which we take to have the square wave form

$$\varepsilon_d(t) = \begin{cases} -|\varepsilon_d|, & 0 < t < \dfrac{T}{2}, \\ +|\varepsilon_d|, & \dfrac{T}{2} < t < T, \end{cases} \quad (11)$$

with driving period T. We choose a piecewise constant Hamiltonian for numerical reasons: in this case Eq. (8) can be made exact by choosing Δt such that $T/2$ is a multiple of Δt. We consider time evolution starting from a product state

$$|\Psi(t=0)\rangle = |\Psi_0\rangle_d \otimes |\text{FS}\rangle_{\rm bath}, \quad (12)$$

where $|\text{FS}\rangle_{\rm bath}$ is a half-filled Fermi sea of the bath as shown in Fig. 1. We will provide physical results that show the local quantities on the d-orbital and complexity results that show the growth of entanglement entropy of the bath MPSs at the maximum entropy bond, which is often the one closest to the Fermi level.

III. NONINTERACTING RESULTS

We first present results obtained for the noninteracting driven SIAM using a standard Slater-determinant-based method. The time-evolution of a Slater determinant by a noninteracting Hamiltonian is numerically inexpensive and is not limited by the growth of entanglement entropy.

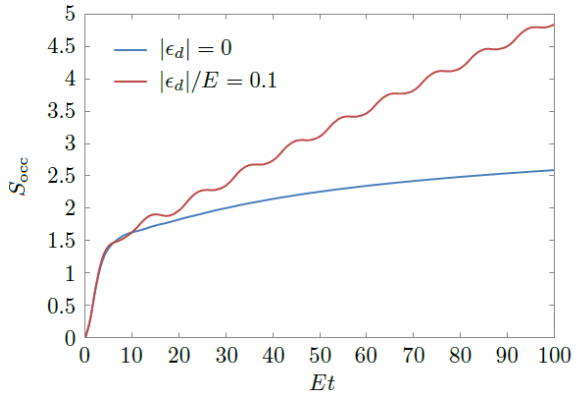

FIG. 2. (Color online) Comparison of time dependence of entanglement entropy of quenched (lower curve, blue online) and driven (upper curve, red online) Anderson impurity model. The driving period $ET = 10$, the Hubbard $U = 0$, the bath is half-filled and the impurity-bath coupling $V/E = 0.25$. Initially the impurity is empty. The entanglement entropy is computed between the 500 bath orbitals below the Fermi level and the rest of the system.

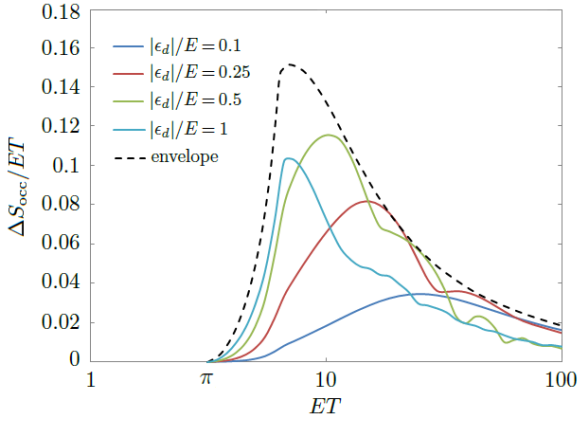

FIG. 3. (Color online) Linear growth rate of entropy over a cycle of the drive in steady state plotted against the driving period for various amplitudes $|\varepsilon_d|$. Hubbard $U = 0$ and the impurity-bath coupling $V/E = 0.25$.

The 4-MPS method will be applied in Sec. IV to obtain results for the interacting model. The impurity-bath coupling in this section is $V/E = 0.25$, and we use $N = 1000$ orbitals. The initial state is $|0\rangle_d \otimes |\mathrm{FS}\rangle_{\rm bath}$, an empty d-orbital and a half-filled Fermi sea in Fig. 1. If ε_d is time-independent, this corresponds to studying the behavior after a quench of ε_d from a very high value.

A. Energy-ordered bath

We use the von Neumann entropy $S_{\rm occ} = -\mathrm{Tr}(\rho \ln \rho)$ for the entanglement between the $N/2$ bath orbitals below the Fermi level and the rest of the system to estimate the maximum entanglement entropy that would be encountered in an MPS-based simulation when the bath orbitals are energy-ordered. Figure 2 compares the growth of the entanglement entropy in the quench case (lower curve, blue online) and the driven case (upper curve, red online) for driving periods $T > T_c$ longer than the critical period $T_c = \pi/E$. We see that the entanglement entropy in the quench case grows logarithmically in time, consistent with previous results [20], but in the presence of a periodic drive, the growth of entropy becomes linear in time.

To understand the factors controlling the growth of entanglement entropy in the driven SIAM, we plot in Fig. 3 the increase rate of entanglement entropy per driving period against the dimensionless driving period ET for different values of driving amplitude $|\epsilon_d|$. The results are obtained at long times after the simulation was started and represent the steady-state growth of entanglement entropy. We see that for $ET < \pi$ (i.e., for driving frequency $\omega_d = 2\pi/T$ greater than the full band width $2E$), there is no discernible steady-state linear increase of entropy over one drive period. In other words, the entropy grows more slowly than linearly (in fact, it grows logarithmically) with time. For $ET > \pi$, the steady-state growth rate of entanglement entropy is non-zero, and depends on the driving period and amplitude in a complicated way. The growth rate has a maximum at a drive frequency that depends on the drive amplitude and is always within the envelope shown as the dashed curve, which is obtained by numerically maximizing the linear growth rate $\Delta S_T/T$ of entropy at fixed period T via tuning the amplitude $|\varepsilon_d|$.

The existence of the critical driving period may be understood within Floquet-Magnus theory [21–24], which states that at high driving frequency, periodically driven systems with Hamiltonian $H(t)$ may be represented in terms of a time-independent Hamiltonian $\bar{H}$ with the parameters determined by averages of parameters in $H(t)$ over one driving period. Corrections to the high-frequency limit may be expressed as a power series in the driving period T. If the series converges, the physics of a system in which periodic drive is turned on is in effect that of a quenched model. In the particular case of the SIAM studied here, this would mean that the entanglement entropy increases with time logarithmically. We then interpret the critical period that marks the onset of linear entropy growth as the radius of convergence of the Magnus expansion.

For the noninteracting SIAM, the convergence radius of the Magnus expansion can be determined from the Floquet Hamiltonian H_F, which is defined as the time-independent Hamiltonian whose time-evolution over a full period T reproduces the time-evolution of the driven system over the same period, i.e.,

$$e^{-iH_F T} \equiv \mathcal{T} e^{-i\int_0^T H(t)dt}. \tag{13}$$

For the square-wave model in Eq. (11), the solution for small driving amplitude $|\varepsilon_d|$ can be resummed exactly to

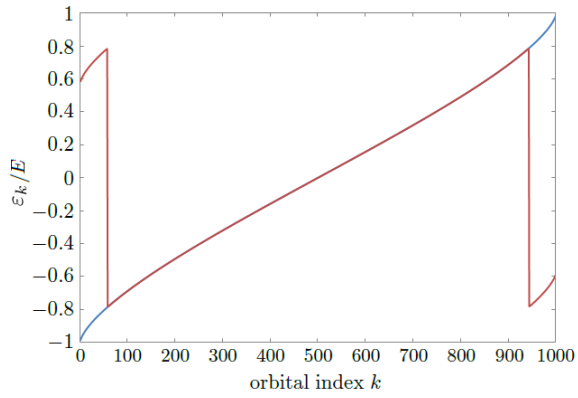

FIG. 4. (Color online) The bath orbital energies ε_k of the Floquet Hamiltonian H_F for $ET = 3$ (blue) and $ET = 4$ (red). The orbital energies are unaffected by the periodic driving if $ET < \pi$ but get aliased to quasi-energies within $[-\pi/T, \pi/T]$ modulo $2\pi/T$ if $ET > \pi$.

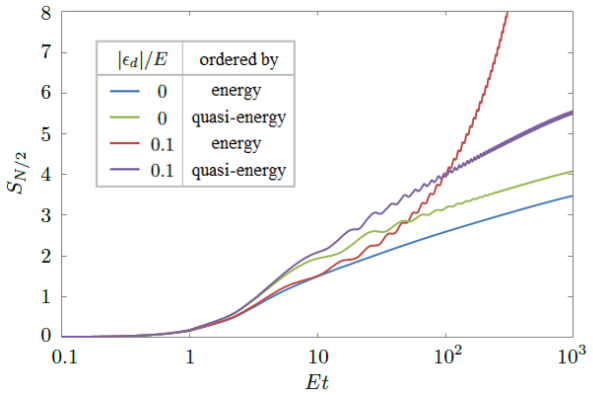

FIG. 5. (Color online) The growth of entropy $S_{N/2}$ for the driven and quenched models with energy-ordered and quasi-energy-ordered bath orbitals. Hubbard $U = 0$ and impurity-bath coupling $V/E = 0.25$. Period $ET = 10$.

find (details in Appendix A)

$$H_F = \bar{H} + i|\varepsilon_d| \tan\left(\frac{T}{4}\,\mathrm{ad}_{\bar{H}}\right) n_d + \mathcal{O}(|\varepsilon_d|^2), \qquad (14)$$

where $\bar{H} = \frac{1}{T}\int_0^T H(t)dt$ is the time-averaged Hamiltonian, $\mathrm{ad}_{\bar{H}} = [\bar{H}, \cdot]$ is the adjoint representation of $\bar{H}$ and the $\tan(\cdot)$ function is defined by its formal power series. In the noninteracting model, the spectral radius of $\mathrm{ad}_{\bar{H}}$ is $2E$ and the expansion of the $\tan(\cdot)$ fails when its argument is $\pi/2$, reproducing the critical value shown in Fig. 3. We expect that very similar considerations will apply to the interacting SIAM.

The linear growth of entanglement entropy in the long-period regime $ET > \pi$ where the Magnus expansion breaks down may be understood in an entropy pumping picture. The up and down motion of the d orbital acts as an elevator that transports electrons from occupied to unoccupied orbitals. For small T this process does not affect the energy ordering and does not lead to entropy increase. For T longer than the convergence radius, the bath orbital energies are aliased to $[-\pi/T, \pi/T] \subset [-E, E]$, breaking the original ordering of the bath orbitals and leading to entropy increase.

B. Quasi-energy-ordered bath

The above analysis suggests that when the drive period $T > T_c$, we should rearrange the bath orbitals in the MPS in ascending order of quasi-energy, i.e., ε_k modulo $2\pi/T$ to within $[-\pi/T, \pi/T]$, as shown in Fig. 4, rather than energy. To test this idea, we again calculate the entropy growth using the Slater-determinant-based non-interacting simulation. The initial state $|0\rangle_d \otimes |\mathrm{FS}\rangle_{\mathrm{bath}}$ in the star geometry remains a product state (an MPS with bond dimension = 1). The entanglement entropy $S_{N/2}$ between the $N/2$ bath orbitals with negative quasi-energies (within $[-\pi/T, 0)$) and the rest of the system will be used to estimate the maximum entanglement entropy encountered in an MPS-based simulation when the bath orbitals are quasi-energy-ordered. The $S_{N/2}$ defined here becomes equivalent to the entanglement entropy S_{occ} used in the previous section if $ET < \pi$, when the bath orbitals are energy-ordered.

Fig. 5 shows the same simulation as in Fig. 2 using $N = 1000$ bath orbitals now ordered by their quasi-energies of $ET = 10$. The entropies of the energy-ordered simulation in Fig. 2 (blue and red lines) are compared with the new results (green and purple lines) in Fig. 5 and the time t is put on log scale. When the bath orbitals are ordered by quasi-energy, the growth of $S_{N/2}$ is logarithmic for both the quenched and driven models. This is because the Floquet Hamiltonian H_F is now energy-ordered, as opposed to the aliased situation in Fig. 4. But the driven model is still harder to simulate than the quenched model, because the slope of the $S_{N/2}$ v.s. $\ln t$ curve is greater for the driven model.

For the quenched model, the steady-state slope of $S_{N/2}$ v.s. $\ln t$ is unchanged when the bath orbitals are quasi-energy-ordered. Only the steady-state intercept is shifted up by a constant $\Delta S_{N/2}$, which is found to be approximately proportional to $\ln(T/T_c)$ (see Fig. 6a). This is the price to pay for not ordering the quenched bath by energy.

For the driven model, the driving period T changes the slope of the $S_{N/2}$ v.s. $\ln t$ curve. Fig. 6b shows how the slope increases from that of the quenched model ($T \to 0$ at fixed $|\varepsilon_d|$ is equivalent to quench) to unboundedly large values proportional to $\ln T$. This indicates that the leading-order term in the entropy $S_{N/2}$ is

$$S_{N/2} \sim c \ln T \ln t, \qquad (15)$$

where c depends on $|\varepsilon_d|$ but is found to be bounded (see Fig. 7). At very large driving amplitude $|\varepsilon_d| \gtrsim E$, the

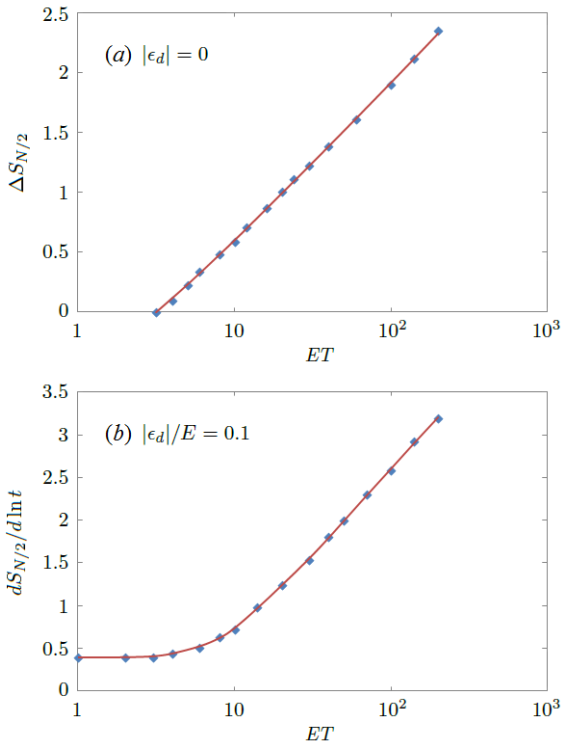

FIG. 6. (Color online) (a) The upshift $\Delta S_{N/2}$ of entropy in the quenched SIAM at $|\varepsilon_d| = 0$ when bath orbitals are ordered by quasi-energy of driving period T. (b) The slope of $S_{N/2}$ v.s $\ln t$ in the driven SIAM at $|\varepsilon_d|/E = 0.1$. Bath size for long periods need to reach $N = 3000$ to obtain accurate data.

coefficient c goes down. The large-$|\varepsilon_d|$ behavior is related to transient formation of bound states as the d-orbital energy moves out of the band.

Eq. (15) means that the bond dimension in an MPS-based simulation using the quasi-energy-ordered bath arrangement is $D \sim e^{S_{N/2}} \sim t^{c \ln T}$. The time complexity of the singular value decomposition (SVD) step is then $\mathcal{O}(D^3) = \mathcal{O}(t^{3c \ln T})$. Since the power of t for the quasi-energy-ordered method is unbounded for long driving periods T, the complexity is still beyond polynomial time. Another drawback of using quasi-energy ordering is the delocalization of maximum entanglement entropy throughout the MPS, while in energy-ordered MPSs, the maximum entanglement entropy tends to concentrate near the Fermi level. This gives the quasi-energy-ordered method a prefactor of the order of the bath size N.

IV. INTERACTING RESULTS

In the previous section, we estimated the growth of entanglement entropy in an MPS-based simulation using a Slater-determinant-based code for the noninteracting SIAM. Now we present MPS-based simulations of the interacting SIAM using the 4-MPS method developed in Sec. II. We choose a fixed Hubbard $U/E = 1$ and

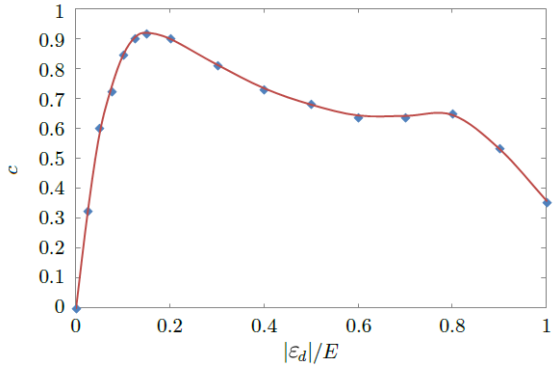

FIG. 7. (Color online) The dependence of the coefficient c in Eq. (15) on the driving amplitude $|\varepsilon_d|$. Hubbard $U = 0$ and impurity-bath coupling $V/E = 0.25$.

the impurity-bath coupling $V/E = 0.25$ is the same as in Sec. III. We use $N = 30$ bath orbitals to fit the hybridization function of the continuum bath DOS in Fig. 1 with good accuracy up to $Et \leq 75$ following [20]. The SVD truncation error tolerance was 10^{-5}. Noninteracting d-occupancies are reproduced with $2 \sim 3$ decimal places as a benchmark.

A. Physical results

For short drive periods $ET < \pi$, we find that the physical results for the driven interacting SIAM are not significantly different from those obtained for the quenched SIAM. So we plot both Figs. 8 & 9 in the long-period regime of $ET > \pi$. The energy-ordered and quasi-energy-ordered algorithms using the 4-MPS method give the same physical result, only costing different CPU times, which will be discussed in Sec. IV B. In Fig. 8, we compare the mean d-occupancy n_d and the double occupancy D computed for the quenched and driven systems. Also shown are the corresponding D values for the noninteracting quenched model in dashed grey line. For period $ET = 10$, both n_d (red line in Fig. 8a) and the double occupancy D (purple line) oscillate approximately sinusoidally, even though the driving signal $\varepsilon_d(t)$ is a square wave: as will be seen, the higher harmonics become noticeable only for higher amplitude of the drive. When the period increases to $ET = 20$, the wave forms approach a relaxed oscillation (Fig. 8b). The overshoots in every period disappear in a noninteracting simulation ($U = 0$, not plotted), which produces simple monotonic decays to the square-wave levels.

When the driving amplitude $|\varepsilon_d|$ is increased, the wave form of n_d distorts, and the relaxation to steady-state oscillation slows down, as is shown in Fig. 9a. Also, there is an increase of double occupancy $\overline{D}$. At $|\varepsilon_d|/E = 0.8$, the steady-state wave form of $D(t)$ is above $n_d^2/4$ almost the entire period. To obtain Fig. 9b, we used the centered moving average method with period equal to the driving

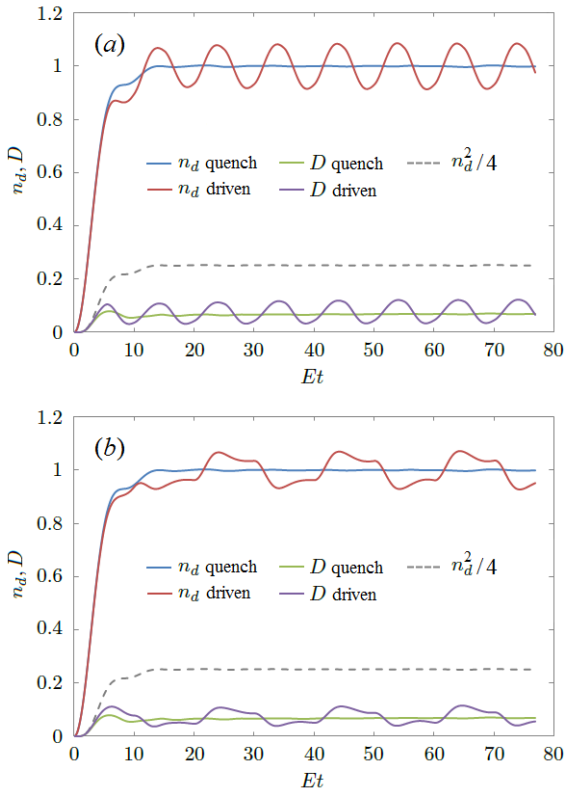

FIG. 8. (Color online) The d-occupancy $n_d = \langle n_{d\uparrow}\rangle + \langle n_{d\downarrow}\rangle$ and double occupancy $D = \langle n_{d\uparrow} n_{d\downarrow}\rangle$ of the quenched and driven SIAMs v.s. time at Hubbard $U/E = 1$, impurity-bath coupling $V/E = 0.25$, driving amplitude $|\varepsilon_d|/E = 0.1$ and period in (a) $ET = 10$ and (b) $ET = 20$. The dashed grey line is $n_d^2/4$ of the quenched n_d.

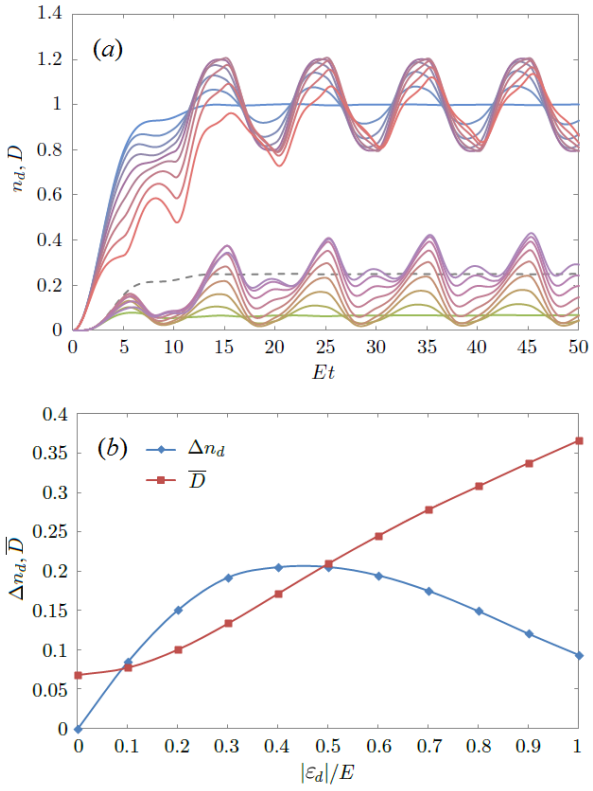

FIG. 9. (Color online) (a) The d-occupancy n_d and double occupancy D of the SIAM at driving amplitudes $|\varepsilon_d|/E = 0, 0.1, \ldots, 0.8$ and period $ET = 10$. Other parameters are the same as Fig. 8. The grey dashed line is $n_d^2/4$ of the quenched n_d. (b) Amplitude Δn_d (1/2 of peak-to-peak value) of n_d and the time-averaged double occupancy $\overline{D}$ over a full period.

period T to obtain the period-averaged quantities $\overline{n_d}(t)$ and $\overline{D}(t)$. Then Δn_d is taken to be half the peak-to-peak value of the oscillatory part $n_d(t) - \overline{n_d}(t)$ of the d-occupancy, and the steady-state $\overline{D}$ is estimated from $\overline{D}(t)$ based on an exponential tail fit. The fit corrects the final value of double occupancy by a non-negligible amount when $|\varepsilon_d|$ is large and the relaxation gets slow.

A possible explanation of the increase of double occupancy $\overline{D}$ might be that the oscillating d-orbital energy is like a phonon mode that induces an effective intra-d-orbital attraction, which becomes greater than U when the amplitude $|\varepsilon_d|$ is big enough ($|\varepsilon_d|/E \gtrsim 0.6$, at which $D \approx 1/4$). Whether this attractive interaction can lead to superconductivity is interesting for further studies.

B. Complexity results

Obtaining results in Fig. 9 at medium to large driving amplitudes required substantial computational resources, because of the slow relaxation to steady state and the rapid growth of entanglement entropy in the $ET > \pi$ regime. In the energy-ordered simulation, the maximum entanglement entropy grows with time linearly, so the maximum bond dimensions in the MPSs increase exponentially with the number of periods simulated. In this section, we investigate whether this exponential difficulty can be helped by reordering the bath orbitals in the MPSs in quasi-energy order.

While the entropy growth in the noninteracting SIAM may be logarithmic in time t if the bath orbitals are ordered by their Floquet quasi-energy, as is shown in Sec. III B, the entropy growth for the interacting SIAM is slightly faster than logarithmic (see red curve in Fig. 10a). We increase the number of bath orbitals to $N = 40$ to reach $Et = 100$, and then compare the energy-ordered and quasi-energy-ordered simulations in Fig. 10 under $|\varepsilon_d|/E = 0.1$, $ET = 6$. As is shown in Fig. 10b, the quasi-energy-ordered 4-MPS simulation is slower in the short run. The short-term growth of entropy, e.g. in the first few periods, is faster if the bath orbitals are not energy-ordered. In the long run, the quasi-energy ordering is more favorable. The entropy growth only slightly curves up in the $S_{\max}$ v.s. $\ln t$ plot. The long-term growth rate of entropy and $\ln t_{\mathrm{CPU}}$ v.s. t are clearly reduced. The difficulty in the $ET > \pi$ regime is beyond

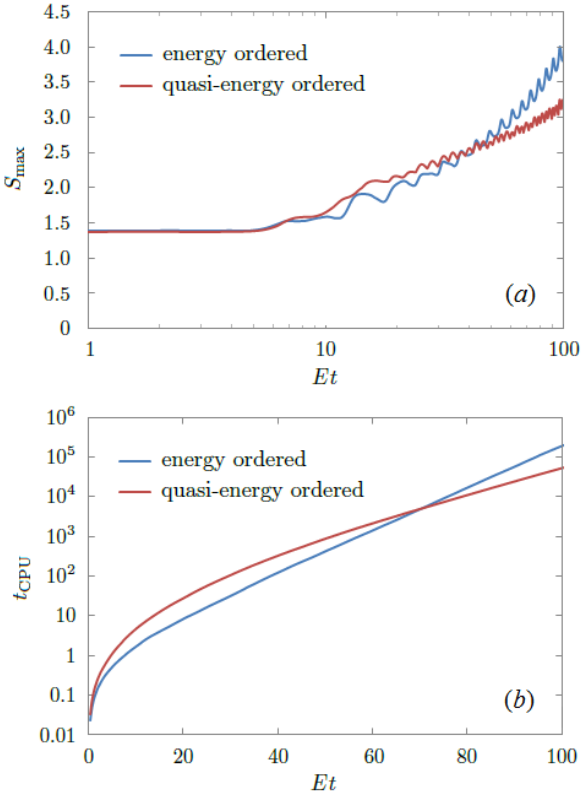

FIG. 10. The maximum entanglement entropy $S_{\max}$ reached in (a) and CPU time t_{CPU} spent in (b) to run to different simulation times Et. Parameter values $U/E = 1$, $V/E = 0.25$, $|\varepsilon_d|/E = 0.1$, and $ET = 6$. The red curve in (a) is slightly concave upward as Et approaches 100 when the period-ET oscillations are eliminated by moving average.

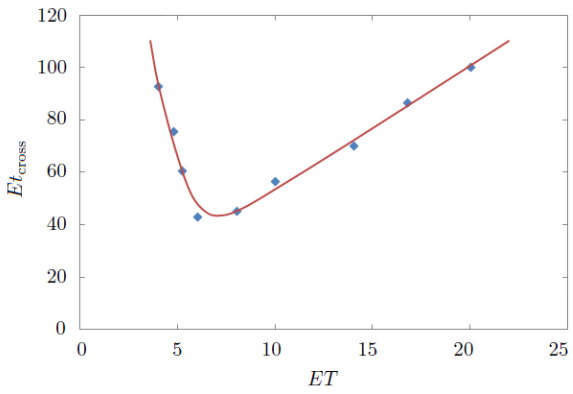

FIG. 11. Crossing time of maximum entanglement entropies of the energy-ordered and quasi-energy-ordered simulations at various driving periods T. Fixed parameter values $U/E = 1$, $V/E = 0.25$, $|\varepsilon_d|/E = 0.1$. The red line is a smooth guideline of the data points in blue dots.

polynomial time using either method, but is significantly reduced by the quasi-energy ordering method.

Figure 11 shows the crossing time of the maximum entanglement entropies $S_{\max}$ of the energy-ordered and quasi-energy-ordered simulations. In a wide range of driving periods, the crossing time t_{cross} of the entropies in Fig. 10 exists and is minimum at intermediate driving periods T at which the linear growth rate of entropy $S_{\max}$ of the energy ordering method is fastest. After the entropies cross, the quasi-energy ordering method still needs to overcome two more short-term drawbacks: a) its maximum entanglement entropy is widely spread over the MPS bonds, in contrast to the energy ordering method, where the entanglement entropy is concentrated near the Fermi level, and b) the bigger entropy in the first few periods, before the CPU-times cross.

V. CONCLUSION

This paper presents a generalization of our previously developed 4-MPS method to time-dependent Hamiltonians and uses the formalism to study the driven SIAM. We analyzed the computational time complexity in the short drive-period $ET < \pi$ and the long-drive period $ET > \pi$ regimes for both the noninteracting ($U = 0$) and interacting ($U > 0$) models. The behavior of the driven model in the $ET < \pi$ regime, where the Floquet-Magnus expansion converges, is not significantly different from the quenched model, either in terms of computational complexity (both requiring only polynomial time) or physical results. However, in the $ET > \pi$ regime, the entropy grows linearly in the energy-ordered algorithm. The long times (many periods) are therefore exponentially hard to reach. Ordering the bath orbitals by quasi-energy reduces the entropy growth of the noninteracting model from linear to logarithmic, albeit with a coefficient of the logarithm that grows unboundedly with the drive period T (proportional to $\ln T$). For the interacting model, quasi-energy ordering significantly reduces the linear growth rate of entanglement entropy and thus the exponential hardness grows with time more slowly in the long run.

The Floquet Hamiltonian of an interacting lattice system outside the convergence radius of the Floquet-Magnus expansion can exhibit highly rich and nontrivial behavior, as is shown in [23, 25]. The work presented here shows that the growth of entanglement entropy depends strongly on basis. A quasi-energy ordering of bath orbitals in the MPS as motivated by the Floquet Hamiltonian of the noninteracting SIAM can reduce the computational complexity, but we have no reason to believe the basis sets studied here are optimal. Further research into the basis sets of the matrix product states based on more refined analyses of the Floquet Hamiltonians for driven interacting models could be an interesting direction for future studies.

Acknowledgments: This research is supported by the Department of Energy under grant DE-SC0012375.

Appendix A: Floquet Hamiltonian

The Floquet Hamiltonian H_F of a periodically driven system $H(t) = H_0 + \epsilon H_1(t)$ is given by

$$e^{-iH_F T} = \mathcal{T} e^{-i\int_0^T dt\,[H_0+\epsilon H_1(t)]}. \tag{A1}$$

For small amplitudes we have $\epsilon \to 0$. We can take derivative with respect to ϵ at $\epsilon = 0$ to obtain

$$\mathcal{T} e^{-i\int_0^T dt\,[H_0+\epsilon H_1(t)]} = e^{-iH_0 T} - i\epsilon \int_0^T dt\, e^{-iH_0(T-t)} H_1(t) e^{-iH_0 t} + \mathcal{O}(\epsilon^2). \tag{A2}$$

We define an expansion

$$H_F = H_0 + \epsilon\, \delta H_F^{(1)} + \mathcal{O}(\epsilon^2). \tag{A3}$$

Then we have

$$e^{-iH_F T} = e^{-i(H_0+\epsilon\,\delta H_F^{(1)})T} + \mathcal{O}(\epsilon^2) = e^{-iH_0 T} - i\epsilon \int_0^T dt\, e^{-iH_0(T-t)}\, \delta H_F^{(1)} e^{-iH_0 t} + \mathcal{O}(\epsilon^2). \tag{A4}$$

Comparing Eqs. (A2) and (A4), we have from the first-order terms of ϵ that

$$\int_0^T dt\, e^{iH_0 t} H_1(t) e^{-iH_0 t} = \int_0^T dt\, e^{iH_0 t}\, \delta H_F^{(1)} e^{-iH_0 t}, \tag{A5}$$

where we have multiplied on both sides by $e^{iH_0 T}$ from the left. Then we use the nested commutator expansion

$$e^{iH_0 t} H_1(t) e^{-iH_0 t} = \sum_{n=0}^{\infty} \frac{(it)^n}{n!}\, \mathrm{ad}_{H_0}^n [H_1(t)], \tag{A6}$$

where $\mathrm{ad}_{H_0} \equiv [H_0, \cdot]$ is the adjoint representation of H_0, and $\mathrm{ad}_{H_0}^n [H_1(t)] = [H_0, \mathrm{ad}_{H_0}^{n-1}[H_1(t)]]$ is the n-fold nested commutator of H_0 with $H_1(t)$. Using this formula on both sides of Eq. (A5), and from the square-wave model

$$H_1(t) = H_1 \,\mathrm{sgn}\left(t - \frac{T}{2}\right), \quad 0 \le t < T, \tag{A7}$$

we obtain the series expansion

$$\sum_{n=0}^{\infty} \frac{(iT)^n}{(n+1)!} \left(1 - \frac{1}{2^n}\right) \mathrm{ad}_{H_0}^n (H_1) = \sum_{n=0}^{\infty} \frac{(iT)^n}{(n+1)!}\, \mathrm{ad}_{H_0}^n (\delta H_F^{(1)}), \tag{A8}$$

which can be resummed to yield

$$\frac{(e^{i\frac{T}{2}\mathrm{ad}_{H_0}} - 1)^2}{iT\mathrm{ad}_{H_0}}\, H_1 = \frac{e^{iT\mathrm{ad}_{H_0}} - 1}{iT\mathrm{ad}_{H_0}}\, \delta H_F^{(1)}. \tag{A9}$$

All functions of ad_{H_0} are defined using their power series in Eq. (A8). We now apply the multiplicative inverse of the power series of ad_{H_0} on the right-hand side to both sides and after some algebra obtain

$$\delta H_F^{(1)} = i \tan\left(\frac{T}{4}\,\mathrm{ad}_{H_0}\right) H_1. \tag{A10}$$

The formal solution in Eq. (A10) can be evaluated in the eigenbasis of H_0 as

$$\langle m|\delta H_F^{(1)}|n\rangle = i\langle m|H_1|n\rangle \tan\left(\frac{E_m - E_n}{4} T\right). \tag{A11}$$

where $|m\rangle$ and $|n\rangle$ are eigenstates of H_0 with eigenenergies E_m and E_n. In case $H_1 = |\epsilon_d| n_d$ with $n_d \equiv \sum_\sigma d_\sigma^\dagger d_\sigma$, Eq. (14) in the main text is derived. Since no assumption is made on H_0 except it is time independent, Eqs.(A10), (A11) & (14) hold for both the interacting and the noninteracting SIAMs.

[1] V. M. D. Paoli, S. H. D. P. Lacerda, L. Spinu, B. Ingber, Z. Rosenzweig, and N. Rosenzweig, Langmuir **22**, 5894 (2006).
[2] S. Banerjee and K. Shah, Physics of Plasmas **25**, 042302 (2018).
[3] S. Basak, Y. Chougale, and R. Nath, Phys. Rev. Lett. **120**, 123204 (2018).
[4] J. E. Boschker, R. N. Wang, V. Bragaglia, P. Fons, A. Giussani, L. L. Guyader, M. Beye, I. Radu, A. V. Kolobov, K. Holldack, and R. Calarco, Phase Transitions **88**, 82 (2015), https://doi.org/10.1080/01411594.2014.971322.
[5] W. L. Shaw, A. D. Curtis, A. A. Banishev, and D. D. Dlott, Journal of Physics: Conference Series **500**, 142011 (2014).
[6] P. W. Anderson, Phys. Rev. **124**, 41 (1961).
[7] A. Georges, G. Kotliar, W. Krauth, and M. J. Rozenberg, Rev. Mod. Phys. **68**, 13 (1996).
[8] G. Kotliar, S. Y. Savrasov, K. Haule, V. S. Oudovenko, O. Parcollet, and C. A. Marianetti, Rev. Mod. Phys. **78**, 865 (2006).
[9] C. Gramsch, K. Balzer, M. Eckstein, and M. Kollar, Phys. Rev. B **88**, 235106 (2013).
[10] M. H. Hettler, J. Kroha, and S. Hershfield, Phys. Rev. B **58**, 5649 (1998).
[11] G. Cohen, E. Gull, D. R. Reichman, and A. J. Millis, Phys. Rev. Lett. **115**, 266802 (2015).
[12] K. Balzer, Z. Li, O. Vendrell, and M. Eckstein, Phys. Rev. B **91**, 045136 (2015).
[13] N. Blümer, Phys. Rev. B **76**, 205120 (2007).

[14] S. R. White, Phys. Rev. Lett. **69**, 2863 (1992).
[15] U. Schollwock, Rev. Mod. Phys. **77**, 259 (2005).
[16] G. Kin-Lic Chan and S. Sharma, Annual review of physical chemistry **62**, 465 (2010).
[17] M. A. Cazalilla and J. B. Marston, Phys. Rev. Lett. **88**, 256403 (2002).
[18] S. R. White and A. E. Feiguin, Phys. Rev. Lett. **93**, 076401 (2004).
[19] F. A. Wolf, I. P. McCulloch, and U. Schollwöck, Phys. Rev. B **90**, 235131 (2014).
[20] Z. He and A. J. Millis, Phys. Rev. B **96**, 085107 (2017).
[21] S. Blanes, F. Casas, J. Oteo, and J. Ros, Physics Reports **470**, 151 (2009).
[22] T. Kuwahara, T. Mori, and K. Saito, Annals of Physics **367**, 96 (2016).
[23] M. Bukov, M. Kolodrubetz, and A. Polkovnikov, Phys. Rev. Lett. **116**, 125301 (2016).
[24] S. Vajna, K. Klobas, T. Prosen, and A. Polkovnikov, Phys. Rev. Lett. **120**, 200607 (2018).
[25] L. D'Alessio and M. Rigol, Phys. Rev. X **4**, 041048 (2014).